AIP Journal of Applied Physics

Electrical transport properties and modelling of electrostrictive resonance phenomena in Ba2/3Sr1/3TiO3 thin films

A. Ghalem, L. Huitema, A. Crunteanu, M. Rammal, L. Trupina, L. Nedelcu, M. G. Banciu, P. Dutheil, C. Constantinescu, P. Marchet, F. Dumas-Bouchiat, and C. Champeaux

Citation: Journal of Applied Physics **120**, 184101 (2016); doi: 10.1063/1.4966942
View online: http://dx.doi.org/10.1063/1.4966942
View Table of Contents: http://scitation.aip.org/content/aip/journal/jap/120/18?ver=pdfcov
Published by the AIP Publishing

JOURNAL OF APPLIED PHYSICS **120**, 184101 (2016)

Electrical transport properties and modelling of electrostrictive resonance phenomena in $Ba_{2/3}Sr_{1/3}TiO_3$ thin films

A. Ghalem,[1,a)] L. Huitema,[1] A. Crunteanu,[1] M. Rammal,[1] L. Trupina,[2] L. Nedelcu,[2] M. G. Banciu,[2] P. Dutheil,[3] C. Constantinescu,[3] P. Marchet,[3] F. Dumas-Bouchiat,[3] and C. Champeaux[3]
[1]*XLIM UMR 7252 CNRS/University of Limoges, 87060 Limoges, France*
[2]*National Institute of Materials Physics, 077125 Bucharest-Magurele, Romania*
[3]*University of Limoges, CNRS, SPCTS, UMR 7315, F-87068 Limoges, France*

(Received 6 September 2016; accepted 20 October 2016; published online 9 November 2016)

We present the conduction mechanisms of $Ba_{2/3}Sr_{1/3}TiO_3$ thin films integrated in metal-insulator-metal (MIM) capacitors and the modelling of the frequency-dependent electrostrictive resonances (in the 100 MHz–10 GHz domain) induced in the devices upon applying different voltage biases. Au/BST/Ir MIM structures on MgO substrates have been fabricated and, depending on their specific polarization, we highlighted different conduction mechanisms in the devices. Depending on the dc bias polarity, the conduction current across the material shows a space-charge-limited-current behavior under negative polarization, whereas under positive bias, the conduction obeys an electrode-limited Schottky-type law at the Au/BST interface. The application of an electric field on the device induces the onset of acoustic resonances related to electrostrictive phenomena in the ferroelectric material. We modeled these acoustic resonances over a wide frequency range, by using a modified Lakin model, which takes into account the dispersions of acoustic properties near the lower electrode/thin film interface. *Published by AIP Publishing.*
[http://dx.doi.org/10.1063/1.4966942]

I. INTRODUCTION

$Ba_xSr_{1-x}TiO_3$ (BST) thin films are receiving considerable consideration as high-potential solutions for the conception of tunable devices in the microwaves and even in the millimeter-waves.[1–7] When integrated in capacitive metal-insulator-metal (MIM) structures, BST films are changing their permittivity upon application of DC electric field, resulting in the modification of the overall capacitance of the MIM device with ratios up to 5:1.[8] Different ferroelectric thin layer compositions have been studied in detail.[9–11] These barium contents can impose a specific state of the BST material (in ferroelectric or paraelectric forms) at room temperature.

The research presented in this paper (electrical and high-frequency characterization of BST material integrated in tunable MIM-type varactor devices) is a necessary step for the integration of the presented components in compact and low power consumption high-frequency devices. The final and specific goal is to realize a reconfigurable antenna exploiting the agility of BST materials integrated in MIM devices. The integration of a tunable BST-based capacitance within an antenna will reconfigure its working frequency for wireless communication on the ISM band going from 2.4 GHz to 2.5 GHz. To be competitive with other tunable components, such as AsGa varactor diodes, the BST capacitors need to have low losses while having a good tunability and reliability.[12–14] Two factors are directly influencing both the BST losses and reliability: leakage currents of the MIM capacitances and the onset acoustic resonances at high frequencies. The global understanding and characterisation of these two phenomena are important, and necessary steps are taken for improving the quality of the BST layer in order to obtain the best adapted capacitance value of the devices on the ISM band and, at the same time, the lowest losses in the same frequency band.

Depending on the electrode's type (noble metals, rutile-type oxides, or complex perovskite oxides like $LaNiO_3$ or $SrRuO_3$),[15–17] typical conduction mechanisms proposed for BST thin film capacitors include film/electrodes interface-dominated Schottky emission[18] bulk-related mechanisms like space-charge-limited conduction (SCLC)[19] or Poole-Frenkel conduction,[23] etc. For MIM capacitive structures, the electrode nature is therefore influencing the properties of the devices. Moreover, a variation of both lattice parameter and thermal expansion coefficient between the electrode and the film can cause important variations of dielectric properties and significantly increase the leakage current.[21,22] Thus, interfacial layers between electrodes (the upper and/or the lower one) and the BST film have a significant impact on the degradation of the dielectric BST thin film.[20] The reason for this degradation can be explained by the bias drop across the interface due to the occurrence of a depolarizing field near the electrodes. Indeed, when a dielectric material is submitted to an external electric field, the dipoles induced in the material generate a depolarizing electric field, which tends to oppose the external field and thus contributes to the fall of the polarization at the interfaces.[24–26] Consequently, the interfacial layer shows a much lower permittivity than the rest of the film and can be considered as a series parasitic

[a)]Author to whom correspondence should be addressed. Electronic mail: areski.ghalem@unilim.fr

capacitance, which may greatly reduce the material permittivity and, therefore, the capacitance of the BST device.

In addition to the onset of leakage currents, an acoustic phenomenon occurs when applying DC bias voltages for tuning the BST permittivity within MIM structures. The magnitude of the applied electric fields breaks the central symmetry of the crystal and induces acoustic-type resonance phenomena,[27–30] which are a combination of electrostrictive and piezoelectric effects.[31–34] These bias-induced electrostrictive phenomena are resulting in non-linear effects such as instabilities of the device capacitance and increased losses at specific resonant frequencies in the microwave domain. Although these acoustic resonance phenomena can be appropriately used to develop voltage controlled resonators or filters,[35,36] they may become easily a critical issue for high-frequency applications where losses, stability, and linearity of the agile capacitors are essential.

A better understanding of this phenomenon on a wide frequency range (especially at microwave frequencies) requires to take into account various material properties (thicknesses, permittivity, acoustic velocities and impedances, etc.), as well as device designs (type of electrodes, electrode/BST film interfaces, etc.). Lakin *et al.*[37] developed a convenient analysis of these acoustic resonances induced by polarization fields. The model is using the electrical impedance description of each layer of the ferroelectric MIM capacitance considered as a parallel plate composite resonator. However, so far, the modeling of such acoustic phenomena was performed only for the first acoustic resonance appearing in the device response corresponding to a limited frequency domain.[38]

The present paper focuses on transport properties and mechanisms for the leakage current of asymmetric Au/$Ba_{2/3}Sr_{1/3}TiO_3$/Ir ferroelectric capacitors as well as on the broad frequency band modelling of their electrostrictive behavior at different applied biases. Although there is a significant number of results concerning the electrical properties of the Pt/BST interface,[39–43] the electrical properties of the Ir/BST system (Ir as bottom electrode) are less described in the literature.[14,44]

We also demonstrate that the interfacial Ir electrode/BST film layer plays a fundamental role within the Lakin formalism for properly model the additional secondary harmonic acoustic resonances of the electrostrictive responses in the MIM device, on a broader frequency domain.

II. EXPERIMENTAL PROCEDURE

In order to characterise the electrical transport properties of the BST layers, we fabricated MIM structures and evaluated their current-voltage (I–V) characteristics. The fabrication process starts with the deposition of an optimized iridium bottom electrode (100 nm) by radiofrequency magnetron reactive sputtering, at 600 °C, on a MgO (100) substrate. It follows the deposition of the BST layer by pulsed laser deposition (PLD) from a $Ba_{2/3}Sr_{1/3}TiO_3$ target using a KrF (248 nm) excimer laser with a pulse rate of 10 Hz and a fluence of 4.5 J/cm^2. During deposition, the substrate was kept at 700 °C in oxygen atmosphere (ambient pressure of 0.3 mbar). The deposition time varies between 30 and 60 min with a target-substrate distance of 5 cm, resulting in BST film thicknesses between 200 nm and 1450 nm. Following their deposition, the BST films were structured in square patterns ($100 \times 100\,\mu m^2$) using a photolithography step and wet etching. A 200-nm thick gold (Au) electrode with a 10-nm thick Ti adhesion layer was finally thermally evaporated and patterned by a lift-off process on the top of the BST patterns. The surface of facing top and bottom electrodes is $30\,\mu m \times 30\,\mu m$, and the typical topology of the obtained MIM devices is depicted in Fig. 1.

DC and high-frequency characterization studies of the fabricated ferroelectric devices have been conducted at different temperatures and for different polarization voltages. The DC characterization allows extracting the current-voltage (I -V) characteristics of the MIM devices and was performed using a probe station connected to a Keithley 2612A sourcemeter. The device temperature was controlled using a Peltier module placed underneath. The response of the device in the high frequency domain (100 MHz–10 GHz) was recorded using a Rohde & Schwarz vector network analyser (VNA) by measuring devices' reflection coefficient S_{11} (magnitude and phase) under different electrical fields applied between the top and the bottom electrodes (using a GSG (Ground-Signal-Ground) probe and an external bias Tee). For both the DC and RF measurements, the top gold (Au) electrode was biased either negatively or positively.

III. RESULTS AND DISCUSSION

A. DC electrical conduction mechanisms

The current density through the MIM device is defined as the ratio between the current and the square surface of facing electrodes that can be deduced from the current-voltage measurements and plotted against the applied voltage. The interpretation of current density results reveals the specific conduction mechanisms between a metal (electrodes) and an insulator (BST), which are directly linked to the metal/insulator contact: neutral, blocking, or ohmic. In this framework, two main conduction mechanisms can be distinguished: the conduction mechanism limited by electrodes/film interfaces and the bulk limited conduction mechanism. The first mechanism drives the conduction when the metal/insulator contact is either neutral or blocking, whereas the second mechanism is observed for ohmic contacts.

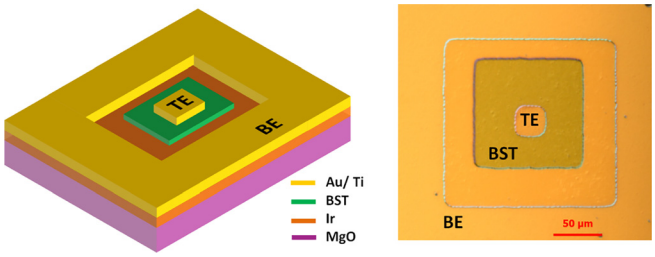

FIG. 1. The schematic view of the fabricated MIM device and the associated optical microscopy top-view image. TE: top electrode, BE: bottom electrode.

The log-log current density as a function of the applied voltage characteristics has been obtained for the I–V measurements performed on a 450 nm-thick BST MIM device, for temperatures and DC bias voltages ranging between 293 K and 333 K and from −4 V to 30 V, respectively.

For negative bias voltages applied to the top Au electrode (with Ir electrode at 20 V), Figure 2(a) shows that the current density is rapidly increasing with the applied voltage. Since current values are limited by the sourcemeter to 1.5 mA (in order to avoid additional heating and current breakdown phenomena in the thin film due to high leakage currents), the value of −4 V is the lowest applied voltage, which could be measured.

In this case, the bias voltage evolution and the temperature dependence can be related to a conduction mechanism limited by the interfaces and particularly to a Schottky emission mechanism.[18] Indeed, the Schottky effect corresponds to an injection of charges in the dielectric by passing above the potential barrier represented by the interface.[45] In this case, the current density that follows a temperature and electrical field evolution was described by the following equation:

$$J = A^{*}T^{2}\exp\left[-\frac{q}{kT}\left(\phi_{B}^{0} - \sqrt{\frac{qE}{4\pi\varepsilon_{0}\varepsilon_{r}}}\right)\right], \quad (1)$$

where A* is the Richardson's constant, T is the temperature, $q\phi_B^0$ is the potential barrier height, E is the applied electric field, and ε_r is the relative dielectric permittivity of the BST material. The application of an electric field reduces the potential barrier and thus favours this type of charge injection.

The Schottky barrier is formed because the metal work function of the gold electrode ($\Phi_{Au} = 5$ eV) is larger than the electron affinity of the BST film ($\chi_{BST} = 4.1$ eV). Consequently, in order to extract the apparent potential barrier at the BST (450 nm)/Au interface, a Schottky mechanism can be considered in the case where the applied bias voltage on the MIM device is negative. Equation (1) can be also expressed as follows:

$$\ln\left(\frac{J}{T^{2}}\right) = \ln(A^{*}) - \frac{q}{kT}\phi_{app}, \quad (2)$$

where $q\Phi_{app}$ is the apparent barrier height, defined according to Equation (3)

$$\phi_{app} = \phi_{B}^{0} - \sqrt{\frac{qE}{4\pi\varepsilon_{0}\varepsilon_{r}}}. \quad (3)$$

The apparent barrier height can be calculated with the slope of the $\ln(J/T^2)$ versus 1000/T representation, which is plotted in Figure 3 for different bias voltages. These plots are reasonably linear in the investigated temperature domain.

The Schottky barrier height is the energy difference between the metal work function of Au and the electron affinity of the BST film and corresponds to the height of barrier that has to cross the charges when passing into the dielectric. It can be obtained by extrapolating the electric field to zero in the description of the apparent barrier height. The dependence of the apparent barrier height on $V^{1/2}$ is represented in the inset of Figure 3.

The extrapolation of the $\Phi_{app} = f(V^{1/2})$ at $V^{1/2} = 0$ allows to extract the Schottky barrier height, with a value of 1.39 eV at the BST/Au interface. This value is in agreement with previous results on similar systems.[46]

The current-voltage evolution is different for a positive polarization (top Au electrode at positive bias and bottom Ir electrode at 0 V, Figure 2(b)). A different conduction mechanism may be clearly noted, and Figure 4 describes the log-log evolution of the current density as a function of the positive electric field for a MIM device integrating a 450-nm BST thick film, at 303 K. We observe that for a low bias voltage, the leakage current densities were below 4×10^{-4} A/cm^2, and the conduction mechanism is ohmic (slope = 1 on Figure 4). Between 3.5 V and 5.5 V, we clearly observe a transition to slope values greater than 1, reflecting a non-ohmic region. Under higher voltages, the log J-log V curve slopes are equal or greater than 2 and define a bulk-type conduction regime, which agrees well with the Space Charge Limited Current—(SCLC) with deep traps mechanism.[18,47]

Indeed, the SCLC theory describes the density current evolution according to the electric field by the relation[48]

$$J = \frac{9\mu\varepsilon_{0}\varepsilon_{r}\theta \cdot E^{2}}{8d}, \quad (4)$$

where ε_r is the relative permittivity of the material, ε_0 is the permittivity of the free space, μ is the mobility, θ is the ratio

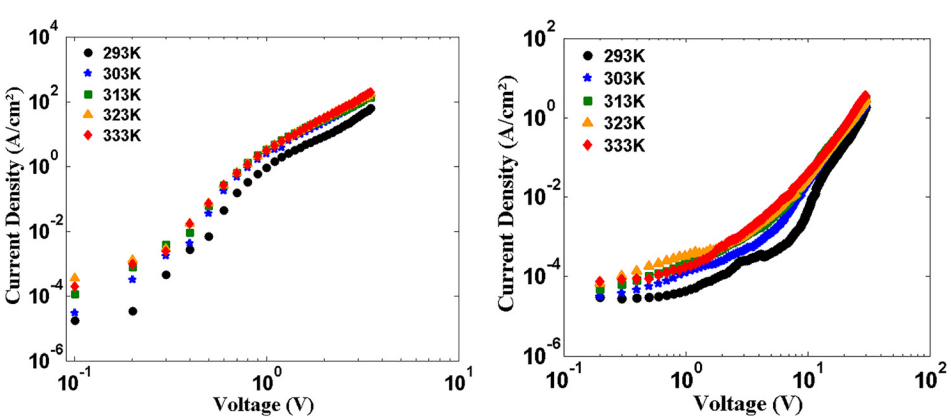

FIG. 2. The log-log representation of current density as a function of bias voltage applied to the top Au electrode for (a) negative and (b) positive bias voltages.

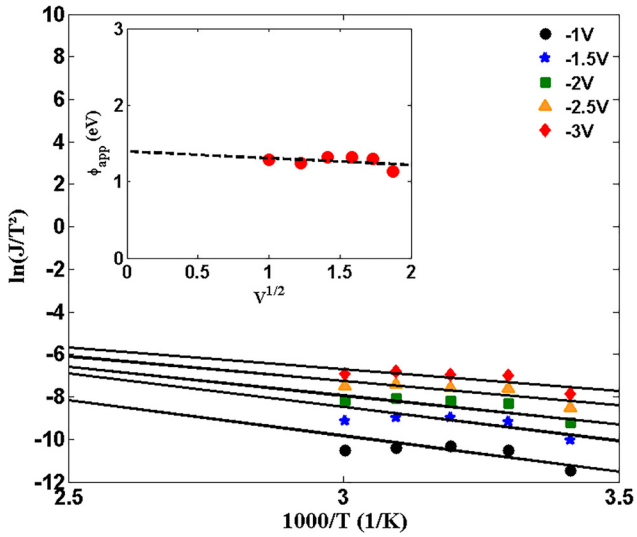

FIG. 3. Ln (J/T^2) representation as the function of 1000/T for different negative bias voltages; inset: Evolution of activation energy as a function of DC bias.

of free-to trapped electric charges, and d is the film thickness.

At low bias voltages, the injected carrier density is negligible compared to the intrinsic carrier density, and the conduction is ohmic (slope equal to 1 in the J-V log-log representation on Figure 4). The SCLC regime occurs when the concentration of the built-in space charge cloud near the injected electrode is negligible against the injected charge density. The current density is following an E^2 dependence described by Equation (4) (slope around 2 in the log-log characteristics).

As the electric field increases up to a voltage threshold (the trap-free voltage limit (V_{TFL})), the amount of the injected charges is increasing and the density of free carriers injected into the active region becomes larger than its intrinsic charge density. Above V_{TFL}, all the trap levels are filled, and the device enters in a different regime (trap-free SCLC or SCLC regime described by different trap level distributions).[47]

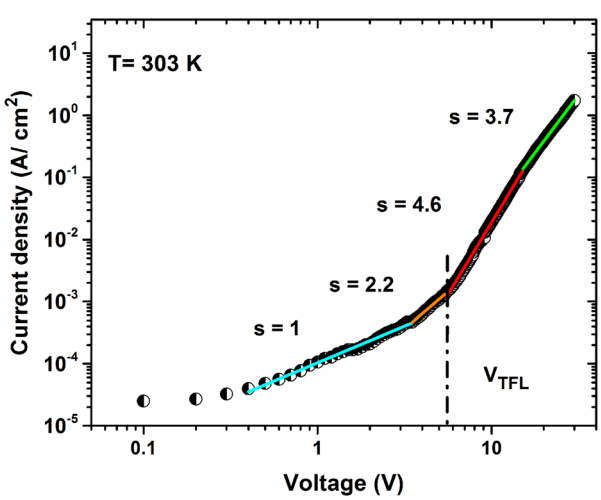

FIG. 4. The log-log plot of the current density vs. the positive bias voltage for the MIM device integrating a 450-nm thick BST film, at 303 K.

If we consider the case of discrete shallow defect levels within the ferroelectric material (for voltages up to V_{TFL}), the density N_t of the trapped charges can be expressed as

$$N_t = \frac{9}{8q}\varepsilon_{r*}\varepsilon_0\frac{V_{TFL}}{d^2}, \tag{5}$$

where q is the charge of electron and V_{TFL} can be experimentally deduced from Figure 4. The extracted value of V_{TFL} is 5.5 V corresponding to an N_t value of $1.7 \times 10^{20}\,cm^{-3}$ at 303 K, which is consistent with previous reports on similar materials.[49]

The trap energy level E_t can be further extracted from the expression of the ratio between the density of free and trapped electrons, θ, which can be expressed as

$$\theta = \frac{N_c \exp[(E_t - E_c)/kT]}{g * N_t}, \tag{6}$$

where N_c is the effective density of states in the conduction band, g is a degeneracy factor (~2), E_c is the energy level of conduction band, k is the Boltzmann constant, and T is the temperature (K). Assuming $N_c = 10^{21}/cm^3$,[14,18,50] we obtain the position of the energy level of traps with respect to the conduction band energy level, E_c-E_t = 0.16 eV, which is in the same order of magnitude with those reported previously.[49]

Taking into account the conduction mechanisms inferred for both negative and positive polarizations, the proposed schematic energy band diagram of the Au/BST/Ir capacitor is presented in Figure 5.

We obtained similar results (analogous conduction mechanisms for an equivalent DC polarization) on MIM devices incorporating BST films with different thicknesses.

B. High-frequency characterization of the MIM devices

After analyzing the electrical characterization of BST thin films and the conduction phenomena at both metal-insulator interfaces, the next part of the paper will focus on the RF characterization of the BST thin films integrated in MIM tunable devices.

From the measurement of MIM devices reflection coefficients S_{11} (magnitude and phase) under different applied voltages, we can extract both the global capacitance and the

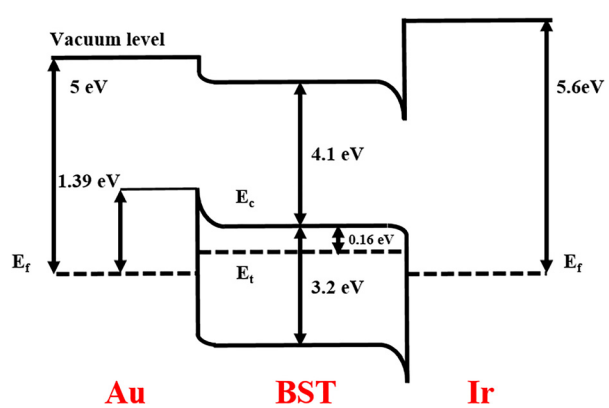

FIG. 5. Energy band diagram of the Au/BST/Ir capacitor.

resistance values[5] according to Equations (7) and (8), respectively,

$$C_{meas} = \frac{1}{\left|Z_0.\omega.\mathrm{Im}\left(\frac{1+S_{11}}{1-S_{11}}\right)\right|}, \tag{7}$$

$$R_{meas} = \mathrm{Re}(Z_{11}) = \mathrm{Re}\left(Z_{0*}\frac{1+S_{11}}{1-S_{11}}\right). \tag{8}$$

The capacitance values variation with the electric field are plotted in Figure 6 for different thicknesses of 200 nm, 450 nm, and 1450 nm for the BST layer. Note that the obtained films are highly oriented and exhibit a (100) preferred orientation with a small (111) contribution. Irrespective of the ferroelectric film thickness, the fabricated $Ba_{2/3}Sr_{1/3}TiO_3$-based MIM devices show extremely high capacitance tuning. The relative capacitance variation goes up to 82% under an electric field as low as 220 kV/cm, which corresponds to an applied voltage of only 10 V for the 450-nm thick MIM device.

The state-of-the-art literature reports presented in Sec. I describe the relationship between the degradation of both the dielectric and acoustic properties of BST films with the presence of an interface layer. This degradation, introduced by the electrode, fo the ferroelectric film interface layer can be quantified by analysing its impact on the overall capacitance of the MIM device. Following the formalism used in Ref. 51, the capacitance measured for the MIM structure (C_{meas}) can be decomposed into the contribution of the BST film and that of the interfacial layer, according to the relationship (9)

$$\frac{1}{C_{meas}} = \frac{1}{C_f} + \frac{1}{C_i}, \tag{9}$$

where C_{meas} corresponds to the measured capacitance and equals $\frac{\varepsilon_0\varepsilon_r S}{d}$ (S is the surface of the opposite electrodes and d is the thickness of the BST layer) and C_i and C_f are the interface and ferroelectric layer capacitances, respectively. If the thickness of the global structure (d) is much higher than one of the interface layers, it can be approximated to the ferroelectric film thickness, i.e., and Equation (9) becomes equivalent to Equation (10)

$$\frac{1}{C_{meas}} = \frac{d}{\varepsilon_0\varepsilon_f S_f} + \frac{1}{C_i}. \tag{10}$$

Therefore, the variation of the characteristic $1/C_{meas} = f(d)$ for MIM structures with different global thicknesses is a straight line whose slope is inversely proportional to the intrinsic dielectric permittivity of the ferroelectric layer, ε_f. Figure 7 describes the evolution of $1/C_{meas} = f(d)$ curve for BST films with different thicknesses of 200 nm, 450 nm, and 1450 nm.

The linear variation of the curve in Fig. 7 is in agreement with the series capacitance model that assumes the existence of regions with degraded dielectric properties close to the lower electrode/ferroelectric interface. Since $1/C_i$ is directly deduced from the y-intercept, we can calculate the interface capacitance, $Ci = 38$ pF. Moreover, the intrinsic permittivity of the BST film (without the contribution of the interface layer) extracted from the slope is $\varepsilon_f = 2220$ and clearly exceeds the overall relative dielectric permittivity ε_r (around 1000) obtained by taking into account the contribution of the interface layer. We can therefore conclude that the interface between an electrode and a BST film contributes to the degradation of the dielectric properties and therefore cannot be disregarded when estimating the accurate dielectric properties of the ferroelectric material.

C. Modelling of the electrostrictive phenomena in the ferroelectric-based MIM device

Fig. 8 shows the measured overall resistance of the tunable device for the 450 nm-thick BST capacitor as a function of the applied voltage. This resistance is equal to the real part of the device input impedance, Z_{11}, extracted from the measurement of reflection parameters S_{11} according to Equation (8). Curves in Fig. 8 exhibit the onset of acoustic-like resonance effects when a DC-bias voltage is applied on the device, called electrostrictive resonances.[5,49,52] Therefore, the resistance values correspond to the global losses of the capacitor device, i.e., including BST film losses, electrodes losses, and electrostrictive effects.

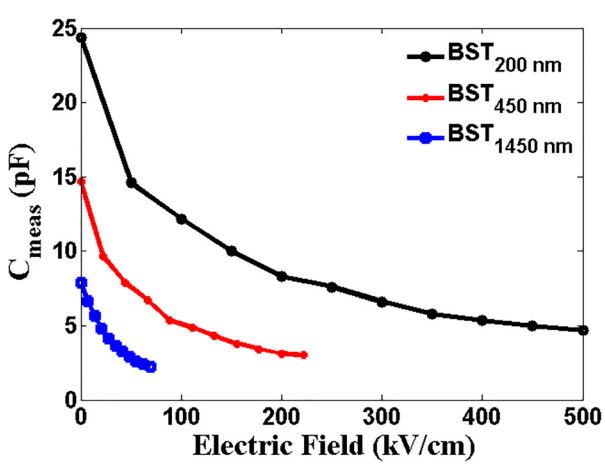

FIG. 6. Capacitance measurement as a function of electric field and for different thicknesses (maximum applied voltage bias of 10 V for all samples).

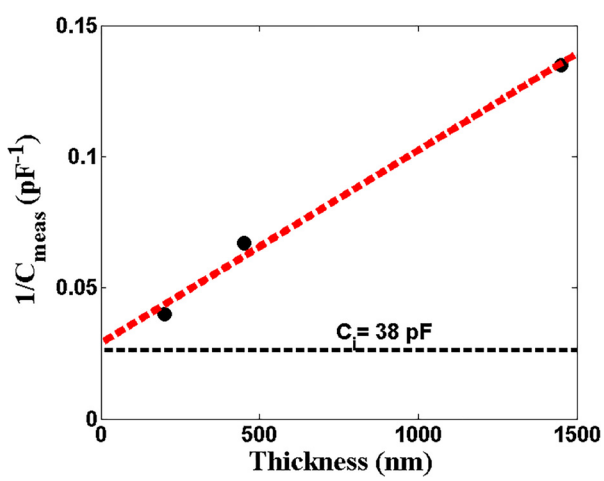

FIG. 7. Evolution of the inverse of capacitance ($1/C_{meas}$) as a function of BST film thicknesses.

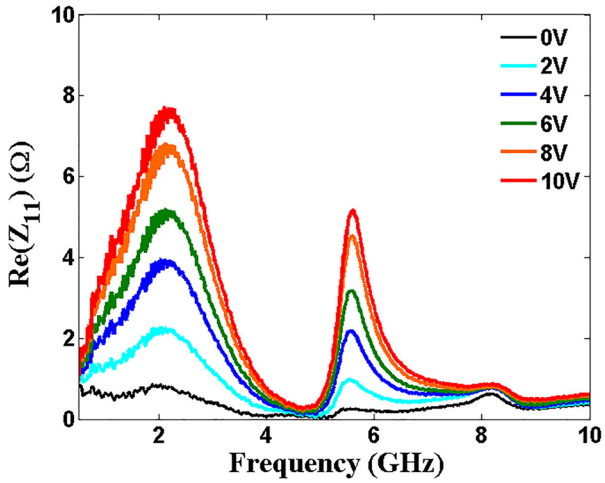

FIG. 8. Frequency evolution of the input impedance Z_{11} as a function of the bias voltage for MIM device integrating a 450-nm thick BST layer.

The electrostrictive resonances are reproducible, and both their resonance frequencies and amplitudes are linked to the BST thickness.[8] Previous reports on these phenomena[33] show that the main electrostrictive resonance is inversely proportional to the BST thickness. However, the knowledge on only the first resonance frequency is not sufficient for the integration of BST materials in practical devices like reconfigurable antennas or filters. Indeed, in the case presented in Fig. 8, the fabricated tunable capacitance could be exploited only on the [3.8 GHz–5.5 GHz] frequency range; since outside this domain, the overall losses are too high. The need to predict the onset and frequency domain of electrostrictive resonance effects is therefore necessary for practical device implementations.

As indicated in the Introduction, the Lakin model[53,54] is a simple and convenient approach for the simulation of an acoustic/electrostrictive behavior of ferroelectric layers integrating in MIM devices. The model is based on the acoustic transmission line transformation by considering the acoustic properties of each constituent layers (substrate, electrodes, and ferroelectric film). The electric impedance of the MIM capacitor is described by the normalized acoustic load impedances z_t and z_b on each side of the ferroelectric thin film sandwiched between the metallic electrodes (Fig. 9).

The equivalent acoustic impedance of the device is described by the following equation:

$$z_{eq} = \frac{1}{jC\omega}\left[1-K^2(V_{DC}) * \frac{\tan\phi}{\phi} \times \left(\frac{(z_t+z_b) * \cos^2\phi + j\sin(2\phi)}{(z_t+z_b) * \cos(2\phi) + j(z_t * z_b + 1)\sin(2\phi)}\right)\right], \quad (11)$$

where ω is the angular frequency, C is the global device capacitance, Φ is the phase over the BST layer defined as $\phi = k.t/2$ where k is the wave vector and t is the BST thickness, K^2 (V_{DC}) is the electromechanical coupling coefficient depending on the applied bias voltage V_{DC}, $z_t = Z_t/Z_{BST}$ and $z_b = Z_b/Z_{BST}$, where Z_{BST} is the acoustic impedance of the BST

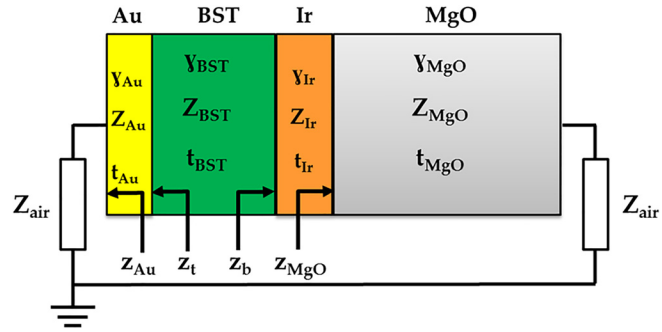

FIG. 9. Equivalent model of the ferroelectric MIM capacitor.

layer while Zt and Z_b are the acoustic impedances of the top and the bottom electrodes interfaces, respectively. Z_t and Z_b are calculated by the classical transmission line equation (12),

$$z_{interface} = z_L\left(\frac{Z_i + Z_L\tanh(\gamma_i t_i)}{Z_L + Z_i\tanh(\gamma_i t_i)}\right), \quad (12)$$

$\gamma_i = \alpha_i + j\beta_i$ is the propagation constant for each layer within the structure, where α_i is the attenuation constant and β_i is the phase constant depending on the acoustic velocity, v_{ac}: $\beta_i = 2\pi f/v_{ac}$. Typical acoustic parameters for each layers comprising the MIM device are described in Table I.

The Lakin acoustic model has been implemented, and Fig. 10 compares the measurement and simulation results of the real part of the Z_{11} parameter for different applied DC bias voltages.

As observed in Figure 10 and already confirmed for similar devices,[38,41] we noticed a good agreement between the implemented model and the experimental results for the main acoustic resonance peak, around 2.3 GHz. However, the current implementation of the model fails to correctly simulate the frequency position of the second acoustic harmonic, which has a significant frequency shift and an important magnitude difference when compared with the measurement results. In order to explain this shift, Vorobiev and Gevorgian[55] discussed the possibility of a frequency dispersion of the acoustic velocity in the ferroelectric material, which would explain in their case the frequency position of the second harmonic resonance.

Following this hypothesis, we further considered introducing an interfacial layer (typically about 10–70 nm) in the electrostrictive model layers stack at the Ir/BST interface, with dissimilar acoustic properties in comparison with the main BST layer.

The different interpretations proposed in the literature consider this interfacial layer as a low permittivity medium

TABLE I. Geometrical and acoustic parameters of the layers considered in the MIM stack.

Material	Thickness (μm)	v_{ac} (m/s)	Z *10^6 (kg/m^{2}s)
Au	0.200	2200	62
BST	0.45	4400	55.1
Ir	0.100	3000	30
MgO	500	8000	28.6

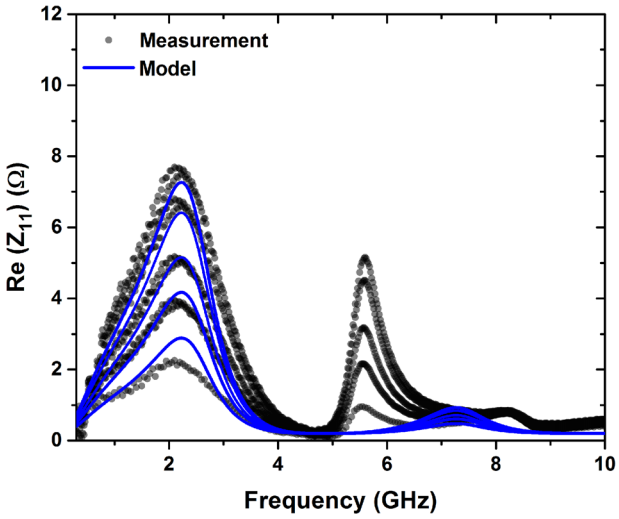

FIG. 10. Frequency evolution of the real part of the input impedance Z_{11} (modelled and measured) for different bias voltages.

and referred to it as an intrinsic layer.[56,57] Moreover, Grossmann *et al.*[58] and Junquera and Ghosez[59] show a suppression of ferroelectric properties in the $Pb(Zr,Ti)O_3$ and $BaTiO_3$ thin films due to the presence of such interfacial layers. Based on the deterioration of the ferroelectric properties at the Ir/BST interface, it is conceivable to also consider a modification of the acoustic properties of this interface layer.

Taking into account all these considerations, the previous electrostrictive model stack was modified (inset in Fig. 11) by introducing an interface layer with optimized acoustic properties (layer thickness of 50 nm with an acoustic velocity of 2200 m/s, around two times less than the acoustic velocity of BST thin films). The comparison of the measurement results and the modelled input impedance of the modified layers stack within the MIM capacitance are represented in Figure 11.

It is obvious from the results presented in Figure 11 that by taking into account an interface layer at the Ir/BST boundary having specific acoustic properties, the electrostrictive resonances induced in the device can be modelled not only for the first resonance peak but also for the successive harmonics, on a larger frequency band.

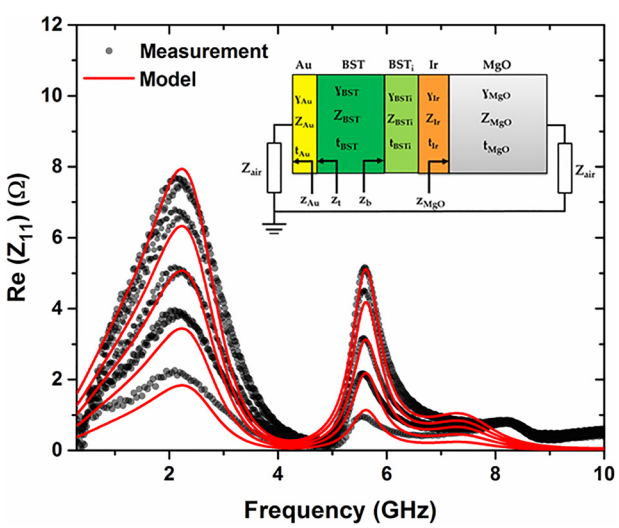

FIG. 11. Frequency evolution of the input impedance (modelled and measured) for different bias voltages considering an equivalent model of the MIM capacitor, which is incorporating an Ir/BST interface layer (inset).

These results are important from the point of view of predicting and evaluating the overall device losses on a larger frequency domain. Indeed, it should be reminded that the real part of the Z_{11} parameter equals the equivalent resistance of the tunable capacitance. Within the radiating element of a tunable antenna, a resistance higher than 2 Ω is not acceptable; therefore, the electrostrictive resonances (frequency positions and amplitude) need to be predicted in order to dismiss them from the working frequency band of the antenna.

The impact of this interfacial layer on the global acoustic properties of ferroelectric MIM devices is still not completely documented, and its real nature remains a subject of discussion in the domain. Nevertheless, different hypotheses have been proposed concerning its origin such as: (i) the destruction of the polarization states near the interface,[54] (ii) the formation of specific conduction mechanisms due to the difference in the band structure between the BST layer and the electrode,[18,60] or (iii) a thin layer adjacent to the electrode with particular microstructure, which behaves like a series capacitor.[61]

The evaluation of the interface layer thickness using the electrostrictive model approach described above allows obtaining further information concerning the dielectric properties of this boundary layer.

In order to have a rough size of the permittivity near the interface, the thickness obtained from the electrostrictive effects simulation was reintroduced in the expressions defining the interface capacitance (Eqs. (9) and (10)). Indeed, from the curve in Figure 7 describing the variation of the BST measured capacitance ($1/C_{meas}$) as a function of the ferroelectric layers thicknesses, we may extrapolate it and extract the Y-intercept of the curve, which defines the capacitance associated with the interface layer (Eq. (13)), which can be expressed as

$$\frac{1}{C_i} = \frac{e_i}{\varepsilon_0 \varepsilon_i S_i}, \tag{13}$$

where C_i is the interface capacitance, e_i, ε_i, and S_i are the thickness, the permittivity, and the surface of the interface layer, respectively. Considering a value of $e_i = 50$ nm, we obtained a permittivity value of $\varepsilon_i \sim 240$, which is significantly lower than that of the BST film. As indicated in Sec. III B, such a small permittivity of the Ir/BST interface layer greatly affects the overall dielectric properties of the ferroelectric BST thin film and the capacitance values of the MIM device. Nevertheless, these results confirm the assumptions concerning the nature of this interface layer, which is expected to have highly dissimilar dielectric properties compared to the ferroelectric film, with a very low permittivity and degraded acoustic and ferroelectric behaviors.[58,62,63] The rigorous simulation of electrostrictive phenomena on a broad frequency domain of such metal/ferroelectric/metal structures must therefore take imperatively into account the

influence of the lower electrode/ferroelectric film interface layer.

IV. CONCLUSION

In this paper, we studied the conduction mechanisms MIM devices integrating a paraelectric $Ba_{2/3}Sr_{1/3}TiO_3$ thin film with a paraelectric behavior at room temperature. The negative and positive polarization of the device allowed determining the conduction laws (Schottky and SCLC, respectively) and the band diagram of the Au/BST/Ir/MgO structure. The analysis of the dielectric properties of the BST films along with the modeling of electrostrictive acoustic resonance phenomena appearing in the MIM devices in the high-frequencies domain indicates the existence of an interface layer at the BST/Ir boundary with dissimilar dielectric and acoustic properties when compared with the BST layer. We demonstrate that the modification of the electrostrictive Lakin model by including this interface layer in the overall layer stack of the device shows an excellent agreement between the modeled and the measured results over a wide frequency range. The modelling results presented here are relevant from the device integration point of view, by predicting and evaluating the overall device losses on a large frequency domain.

ACKNOWLEDGMENTS

This work was financially supported by the "Agence Nationale de la Recherche" (ANR)-France, the France Region Limousin and the National Authority for Scientific Research (ANCS)-Romania, under the MAESTRO project (ANR-13-ISO3-001) and the H2020 European project MASTERS (M-ERA.NET call). This work was financially supported by the "Agence Nationale de la Recherche" (ANR)-France, the France Region Limousin and the National Authority for Scientific Research (ANCS)-Romania, under the MAESTRO project (ANR-13-ISO3-001) and the H2020 European project MASTERS (M-ERA.NET call).

[1]S. Courrèges, B. Lacroix, A. Amadjikpe, S. Phillips, Z. Zhao, K. Choi, A. Hunt, and J. Papapolymerou, "Back-to-back tunable ferroelectric resonator filters on flexible organic substrates," IEEE Trans. Ultrason. Ferroelectr. Freq. Control **57**, 1267 (2010).

[2]R. De Paolis, S. Payan, M. Maglione, G. Guegan, and F. Coccetti, "High-tunability and high- q -factor integrated ferroelectric circuits up to millimeter waves," IEEE Trans. Microwave Theory Tech. **63**, 2570 (2015).

[3]T. Kimura, H. Kobayashi, Y. Kishimoto, H. Kato, M. Inaba, K.-Y. Hashimoto, T. Matsumura, H. Hirano, M. Kadota, M. Esashi, and S. Tanaka, "Bandwidth-tunable filter consisting of SAW resonators and $BaSrTiO_3$ varactors directly fabricated on a $LiTaO_3$ wafer," in IEEE International Ultrasonics Symposium (IUS) (2014).

[4]I. Vendik, V. Pleskachev, E. Zameshaeva, P. Turalchuk, D. Kholodnyak, I. Kolmakova, S. Zubko, I. Munina, V. Turgaliev, M. Sitnikova, M. Odit, X. Wang, N. Li, L. Sun, and Y. He, in Proceedings of the 43rd European Microwave Conference (2013).

[5]G. Subramanyam, M.-W. Cole, N.-X. Sun, T.-S. Kalkur, N.-M. Sbrockey, G.-S. Tompa, X. Guo, C. Chen, S.-P. Alpay, G.-A. Rossetti, Jr., K. Dayal, L.-Q. Chen, and D.-G. Schlom, "Challenges and opportunities for multifunctional oxide thin films for voltage tunable radio frequency/microwave components," J. Appl. Phys. **114**, 191301 (2013).

[6]H. Khassaf, N. Khakpash, F. Sun, N.-M. Sbrockey, G.-S. Tompa, T.-S. Kalkur, and S.-P. Alpay, "Strain engineered barium strontium titanate for tunable thin film resonators," Appl. Phys. Lett. **104**, 202902 (2014).

[7]N.-M. Sbrockey, T.-S. Kalkur, A. Mansour, H. Khassaf, H. Yu, M. Aindow, S.-P. Alpay, and G.-S. Tompa, "Switchable and tunable film bulk acoustic resonator fabricated using barium strontium titanate active layer and Ta_2O_5/SiO_2 acoustic reflector," Appl. Phys. Lett. **109**, 052902 (2016).

[8]A. Ghalem, M. Rammal, L. Huitema, A. Crunteanu, V. Madrangeas, P. Dutheil, F. Dumas Bouchiat, P. Marchet, C. Champeaux, L. Trupina, L. Nedelcu, and M. G. Banciu, "Ultra-High tunability of $Ba_{(2/3)}Sr_{(1/3)}TiO_3$-based capacitors under low electric fields," IEEE Microwave Wireless Compon. Lett. **26**, 504–506 (2016).

[9]H. S. Kim, H. G. Kim, I. D. Kim, K. B. Kim, and J. C. Lee, "High tunability and low-microwave-loss $Ba_{0.6}Sr_{0.4}TiO_3$ thin films grown on high-resistivity Si substrates using TiO_2 buffer layers," Appl. Phys. Lett. **87**, 212903 (2005).

[10]C. L. Chen, H. H. Feng, Z. Zhang, A. Brazdeikis, Z. J. Huang, W. K. Chu, C. W. Chu, F. A. Miranda, F. W. Van Keuls, R. R. Romanofsky, and Y. Liou, "Epitaxial ferroelectric $Ba_{0.5}Sr_{0.5}TiO_3$ thin films for room-temperature tunable element applications," Appl. Phys. Lett. **75**(3), 412–414 (1999).

[11]D. A. Boyd, S. G. Hirsch, C. Hubbard, and M. W. Cole, "BST films grown by metal organic chemical vapor deposition incorporating real-time control of stoichiometry," Integr. Ferroelectr. **111**(1), 17–26 (2009).

[12]D. Levasseur, H.-B. El-Shaarawi, S. Pacchioni, A. Rousseau, S. Payan, G. Guegan, and M. Maglione, "Systematic investigation of the annealing temperature and composition effects on the dielectric properties of sol–gel $Ba_xSr_{1-x}TiO_3$ thin films," J. Eur. Ceram. Soc. **33**, 139–146 (2013).

[13]W.-Y. Hsu, J.-D. Luttmer, R. Tsu, S. Summerfelt, M. Bedekar, T. Tokumoto, and J. Nulman, "Direct current conduction properties of sputtered Pt/$(Ba_{0.7}Sr_{0.3})TiO_3$/Pt thin films capacitors," Appl. Phys. Lett. **66**, 2975 (1995).

[14]C.-S. Hwang, B.-T. Lee, C.-S. Kang, J.-W. Kim, K.-H. Lee, H.-J. Cho, H. Horii, W.-D. Kim, S.-I. Lee, Y.-B. Roh, and M.-Y. Lee, "A comparative study on the electrical conduction mechanisms of $(Ba_{0.5}Sr_{0.5})TiO_3$ thin films on Pt and IrO_2 electrodes," J. Appl. Phys. **83**, 3703 (1998).

[15]T. Kawakubo, S. Komatsu, K. Abe, K. Sano, N. Yanase, and N. Fukushima, "Ferroelectric properties of $SrRuO_3$/(Ba, Sr)TiO_3/$SrRuO_3$ epitaxial capacitor," Jpn. J. Appl. Phys., Part 1 **37**, 5108 (1998).

[16]A. Srivastava, D. Kumar, and R. K. Singh, "$LaNiO_3$ as contact material for (Ba, Sr)TiO_3 dielectric thin films," Electrochem. Solid-State Lett. **2**, 294–296 (1999).

[17]C-M. Chu and P. Lin, "Electrical properties and crystal structures of (Ba,Sr)TiO_3 films and $BaRuO_3$ bottom electrodes prepared by sputtering," Appl. Phys. Lett. **72**, 1241–1243 (1998).

[18]S.-T. Chang and J.-Y. Lee, "Electrical conduction mechanism in high-dielectric-constant $(Ba_{0.5},Sr_{0.5})TiO_3$ thin films," Appl. Phys. Lett. **80**, 655 (2002).

[19]M.-A. Khan, T.-P. Comyn, and A.-J. Bell, "Deposition of $PbTiO_3$ films on Pt/Si substrates using pulsed laser deposition," J. Eur. Ceram. Soc. **28**, 591 (2008).

[20]C.-S. Hwang, "Bulk- or interface-limited electrical conductions in IrO_2/(Ba,Sr)TiO_3/IrO_2 thin film capacitors," J. Mater. Res. **16**, 3476–3484 (2001).

[21]T.-M. Shaw, Z. Suo, M. Huang, E. Liniger, R.-B. Laibowitz, and J.-D. Baniecki, "The effect of stress on the dielectric properties of barium strontium titanate thin films," Appl. Phys. Lett. **75**, 2129 (1999).

[22]S.-Y. Wang, B.-L. Cheng, C. Wang, S.-A. Redfern, S.-Y. Dai, K.-J. Jin, H.-B. Lu, Y.-L. Zhou, Z.-H. Chen, and G.-Z. Yang, "Influence of Ce doping on leakage current in $Ba_{0.5}Sr_{0.5}TiO_3$ films," J. Phys. D: Appl. Phys. **38**, 2253–2257 (2005).

[23]S.-H. Paek, J. Won, K.-S. Lee, J.-S. Choi, and C.-S. Park, "Electrical and microstructural degradation with decreasing thickness of (Ba, Sr)TiO_3 thin films deposited by RF magnetron sputtering," Jpn. J. Appl. Phys., Part 1 **35**, 5757 (1996).

[24]Y. Wang, M.-K. Niranjan, K. Janicka, J.-P. Velev, M.-Y. Zhuravlev, S.-S. Jaswa, and E.-Y. Tsymbal, "Ferroelectric dead layer driven by a polar interface," Phys. Rev. B **82**, 094114 (2010).

[25]N.-A. Spaldin, "Fundamental size limits in ferroelectricity," Science **304**, 1606 (2004).

[26]R.-R. Mehta, B.-D. Silverman, and J.-T. Jacobs, "DC bias dependent shift of resonance frequencies in BST thin film membranes," *IEEE International Symposium on the Applications of Ferroelectrics* (2007), pp. 236–238.

[27]A. Noeth, T. Yamada, V. Sherman, P. Muralt, A. Tangantsev, and N. Setter, "Tuning of direct current bias-induced resonances in

micromachined $Ba_{0.3}Sr_{0.7}TiO_3$ thin-film capacitors," J. Appl. Phys. **102**, 114110 (2007).
[28]A. Vorobiev, S. Gevorgian, N. Martirosyan, M. Löffler, and E. Olsson, "Intrinsically tunable $_{0.67}BiFeO_3$-$_{0.33}BaTiO_3$ thin film bulk acoustic wave resonators," Appl. Phys. Lett. **101**, 232903 (2012).
[29]S. Gevorgian, A. Vorobiev, and T. Lewin, "DC field and temperature dependent acoustic resonances in parallel-plate capacitors based on $SrTiO_3$ and $Ba_{0.25}Sr_{0.75}TiO_3$ films: Experiment and modeling," J. Appl. Phys. **99**, 124112 (2006).
[30]A. Noeth, T. Yamada, A.-K. Tagantsev, and N. Setter, "Electrical tuning of dc bias induced acoustic resonances in paraelectric thin films capacitors," J. Appl. Phys. **104**, 094102 (2008).
[31]S. Tappe, U. Bottger, and R. Waser, "Electrostrictive resonances in $Ba_{0.7}Sr_{0.3}TiO_3$ thin films at microwave frequencies," Appl. Phys. Lett. **85**, 624 (2004).
[32]W.-P. Mason and B.-T. Matthias, "Theoretical model for explaining the ferroelectric effect in barium titanate," Phys. Rev. **74**, 1622 (1948).
[33]X. Zhu, J. D. Phillips, and A. Mortazawi, "A DC voltage dependent switchable thin film bulk wave acoustic resonator using ferroelectric thin film," *2007 IEEE MTT-S International Microwave Symposium Digest* (2007), pp. 671–674.
[34]W.-P. Mason, "An electromechanical representation of a piezoelectric crystal used as a transducer," Proc. Institute Radio Eng. **23**, 1252–1263 (1935).
[35]M. Schreiter, R. Gabl, D. Pitzer, R. Primig, and W. Wersing, "Electroacoustic hysteresis behaviour of PZT thin film bulk acoustic resonators," J. Eur. Ceram. Soc. **24**, 1589–1592 (2004).
[36]P.-B. Kirby, Q.-X. Su, E. Kornuro, Q. Zhang, M. Imura, and R.-W. Whatmore, "PZT thin film bulk acoustic wave resonators and filters," *IEEE International Frequency Control Symposium and PDA Exhibition* (2001), pp. 687–694.
[37]K.-M. Lakin, G.-R. Kline, and K.-T. Carron, "High-Q microwave acoustic resonators and filters," IEEE Trans. Microwave Theory Tech. **41**, 2139–2146 (1993).
[38]I. Vendik, P.-A. Turalchuk, O.-G. Vendik, and J. Berge, "Modeling tunable bulk acoustic resonators based on induced piezoelectric effect in $BaTiO_3$ and $Ba_{0.25}Sr_{0.75}TiO_3$ films," J. Appl. Phys. **103**, 014107 (2008).
[39]A. Vorobiev, J. Berge, S. Gevorgian, M. Löffler, and E. Olsson, "Effect of interface roughness on acoustic loss in tunable thin film bulk acoustic wave resonators," J. Appl. Phys. **110**, 024116 (2011).
[40]D. Levasseur, E. Bouyssou, R. De Paolis, A. Rousseau, F. Coccetti, G. Guegan, S. Payan, and M. Maglione, "Systematic tuning of the conduction mechanisms in ferroelectric thin films," J. Phys.: Condens. Matter **25**, 495901 (2013).
[41]B. Ivira, A. Reinhardt, E. Defay, and M. Aid, "Integration of electrostrictive $Ba_{0.7}Sr_{0.3}TiO_3$ thin films into bulk acoustic wave resonator for RF-frequency tuning under DC bias," *IEEE International Frequency Control Symposium* (2008), pp. 254–258.
[42]A.-G. Altynnikov, A.-G. Gagarin, M.-M. Gaidukov, A. Tumarkin, P.-K. Petrov, N. Alford, and A.-B. Kozyrev, "Suppression of slow capacitance relaxation phenomenon in Pt/$Ba_{0.3}Sr_{0.7}TiO_3$/Pt thin film ferroelectric structures by annealing in oxygen atmosphere," Appl. Phys. Lett. **104**, 042903 (2014).
[43]K-H. Ahn, S-S. Kim, and S. Baik, "Change of conduction mechanism by microstructural variation in Pt/(Ba,Sr)TiO_3/Pt film capacitors," J. Appl. Phys. **92**, 421–425 (2002).
[44]B. Mešić and H. Schroeder, "Integration of perovskite oxide dielectrics into complementary metal–oxide–semiconductor capacitor structures using amorphous TaSiN as oxygen diffusion barrier," J. Appl. Phys. **110**, 064117 (2011).
[45]L. Pintilie, I. Vrejoiu, D. Hesse, G. LeRhun, and M. Alexe, "Ferroelectric polarization-leakage current relation in high quality epitaxial Pb(Zr,Ti)O_3," Phys. Rev. B **75**, 104103 (2007).
[46]J. Shin, J. Park, C.-S. Hwang, and H.-J. Kim, "Dielectric and electrical properties of sputter grown (Ba,Sr)TiO_3 thin films," J. Appl. Phys. **86**, 506 (1999).
[47]J. Sun, X.-J. Zheng, W. Yin, M. H. Tang, and W. Li, "Space-charge-limited leakage current in high dielectric constant and ferroelectric thin films considering the field-dependent permittivity," Appl. Phys. Lett. **97**, 242905 (2010).
[48]S. M. Sze, *Physics of Semiconductor Device*, 2nd ed. (Wiley, New York, 1981).
[49]C.-J. Peng and S.-B. Krupanidhi, "Structures and electrical properties of barium strontium titanate thin films grown by multi-ion-beam reactive sputtering technique," J. Mater. Res. **10**, 708–726 (1995).
[50]T. Baiatu, R. Waser, and K.-H. Härdt, "DC electrical degradation of perovskite-type titanates: III, A model of the mechanism," J. Am. Ceram. Soc. **73**, 1663–1673 (1990).
[51]R. Bouregba, G. Le Rhun, G. Poullain, and G. Leclerc, "Investigation of thickness dependence of the ferroelectric properties of Pb($Zr_{0.6}Ti_{0.4}$) thin-film capacitors," J. Appl. Phys. **99**, 034102 (2006).
[52]S. Gevorgian, A. Vorobiev, and J. Berge, "Electromechanical modelling and reduction of the electroacoustic losses in parallel-plate ferroelectric varactors," in *Proceeding of the 36th European Microwave Conference* (2006), pp. 851–853.
[53]K-M. Lakin, "Modeling of Thin Film Resonators and Filters," IEEE MTT-S International Microwave Symposium Digest **1**, pp 149–152 (1992).
[54]K. M. Lakin, "Thin film resonator technology," IEEE Trans. Ultrason. Ferroelectr. Freq. Control **52**(5), 707–716 (2005).
[55]A. Vorobiev and S. Gevorgian, "Composite ferroelectric FBARS that are switchable between the first and second harmonics: Experimental demonstration," IEEE Trans. Ultrason. Ferroelect. Freq. Control **62**(3), 565–575 (2015).
[56]C. Zhou and D.-M. Newns, "Intrinsic dead layer effect and the performance of ferroelectric thin film capacitors," J. Appl. Phys. **82**, 3081 (1997).
[57]K. Natori, D. Otani, and M. Sano, "Thickness dependence of the effective dielectric constant in a thin film capacitor," Appl. Phys. Lett. **73**, 632 (1998).
[58]M. Grossmann, O. Lohse, D. Bolten, U. Boettger, T. Schneller, and R. Waser, "Interface-related decrease of the permittivity in $PbZr_xTi_{1-x}O_3$ thin films," Appl. Phys. Lett. **80**, 1427 (2002).
[59]J. Junquera and P. Ghosez, "Critical thickness for ferroelectricity in perovskite ultrathin films," Lett. Nat. **422**, 506 (2003).
[60]C.-S. Hwang, B.-T. Lee, C.-S. Kang, K.-H. Lee, H. Cho, H. Hideki, W.-D. Kim, S.-I. Lee, and M.-Y. Lee, "Depletion layer thickness and Schottky type carrier injection at the interface between Pt electrodes and (Ba, Sr)TiO_3 thin films," J. Appl. Phys. **85**, 287 (1999).
[61]C. Basceri, S.-K. Streiffer, A.-I. Kingon, and R. Waser, "The dielectric response as a function of temperature and film thickness of fiber-textured (Ba,Sr)TiO_3 thin films grown by chemical vapor deposition," J. Appl. Phys. **82**, 2497–2504 (1997).
[62]A. A. Sirenko, C. Bernhard, A. Golnik, A. M. Clark, J. Hao, W. Si, and X. X. Xi, "Soft-mode hardening in $SrTiO_3$ thin films," Lett. Nat. **404**, 373–376 (2000).
[63]C.-T. Black and J.-J. Welser, "Electric-field penetration into metals: Consequences for high-dielectric-constant capacitors," IEEE Trans. Electron. Devices **46**, 776–780 (1999).